

See discussions, stats, and author profiles for this publication at: <https://www.researchgate.net/publication/282723715>

A wavelet–artificial intelligence fusion approach (WAIFA) for blending Landsat and MODIS surface temperature

Article in *Remote Sensing of Environment* · November 2015

DOI: 10.1016/j.rse.2015.08.015

CITATIONS

39

READS

498

5 authors, including:



Vahid Moosavi
Tarbiat Modares University

24 PUBLICATIONS 744 CITATIONS

[SEE PROFILE](#)



Ali Talebi
Yazd University

63 PUBLICATIONS 415 CITATIONS

[SEE PROFILE](#)



Mohammad Hossein Mokhtari
27 PUBLICATIONS 137 CITATIONS

[SEE PROFILE](#)



Seyed Rashid Fallah Shamsi
Shiraz University

51 PUBLICATIONS 381 CITATIONS

[SEE PROFILE](#)

Some of the authors of this publication are also working on these related projects:



I am working on a Haloventure mega project in Bushehr [View project](#)



zoning selected multiple ecosystem services based on spatial patterns of landscape in central part of Isfahan province, Iran [View project](#)



A wavelet-artificial intelligence fusion approach (WAIFA) for blending Landsat and MODIS surface temperature



Vahid Moosavi ^{a,*}, Ali Talebi ^a, Mohammad Hossein Mokhtari ^b, Seyed Rashid Fallah Shamsi ^c, Yaghoub Niazi ^a

^a Department of Watershed Management Engineering, Faculty of Natural Resources, Yazd University, Iran

^b Faculty of Natural Resources, Yazd University, Iran

^c Department of Natural Resources engineering and Environmental Sciences, College of Agriculture, Shiraz University, Iran

ARTICLE INFO

Article history:

Received 18 March 2015

Received in revised form 22 June 2015

Accepted 13 August 2015

Available online xxxx

Keywords:

Artificial intelligence

Data fusion

Land surface temperature

Thermal infrared data

Wavelet transform

ABSTRACT

Land surface temperature (LST) is one of the key parameters in the physics of earth surface processes from local to global scales. However, thermal infrared (TIR) images at both high temporal and spatial resolutions are limited because of the technical limitations of current thermal sensors. Therefore, development of fusion models to obtain thermal data in high spatial and temporal resolutions is crucial in environmental studies. This paper presents a hybrid wavelet-artificial intelligence fusion approach (WAIFA) to produce LST data at the spatial resolution of Landsat 8 thermal bands. The theoretical basis and the application procedures of the proposed data fusion approach are explained. A case study was performed to predict LSTs of six dates in 2014 from March to August in East Azerbaijan Province, Iran. This approach uses powerful non-linear artificial intelligence modeling systems which can cope with the non-linear nature of the land surface temperature data. In addition, multispectral bands and different spectral indices are used as well as thermal data in the modeling process to consider the mixture properties of MODIS pixels. Using a 2D wavelet transform to capture the properties of the main signals (original bands) in horizontal, vertical, and diagonal directions to consider the effect of neighboring pixels is the other improvement of this modeling approach. It can also help the model to deal with the non-stationary properties of the satellite and land surface temperature data. The results indicated that the prediction accuracy of the model in different dates varies from 0.47 K to 1.93 K.

© 2015 Elsevier Inc. All rights reserved.

1. Introduction

Land surface temperature (LST) is one of the main biophysical variables derived from remotely sensed imagery (Anderson et al., 2008). It is widely used for environmental studies such as assessing crop growth (Abuzar, O'Leary, & Fitzgerald, 2009), monitoring vegetation health (Karnieli et al., 2006), agricultural studies (Badeck et al., 2004; Rojas, Vrieling, & Rembold, 2011), estimation of surface energy flux (Muramatsu, Nakayama, & Kaihotsu, 2006), forest burnt area estimation (Ichoku et al., 2003), monitoring evapotranspiration (Anderson, Allen, Morse, & Kustas, 2012; Yang & Wang, 2011) water stress in croplands (Dragutin & Eitzinger, 2007), energy balance (GriendV.D. & Owe, 1993), drought (Karnieli et al., 2010; Sobrino, Gomez, Munoz, & Olioso, 2007) and soil moisture (Hulley, Hook, & Baldridge, 2010). Acquiring satellite images with high temporal and spatial resolutions remains extremely difficult due to satellite technical constraints. It means that thermal imagery with temporal resolution of 1–2 days or less has a moderate to coarse spatial resolution and those with high spatial resolution are limited and are with temporal resolution of more than 15 days (Agam, Kustas, Anderson, Li, & Neale, 2007; Jeganathan et al.,

2011). For example Landsat produces very useful information (from the aspect of spatial resolution), but the 16-day revisit cycle limited its application in detecting rapid surface changes such as crop-growth, evaporation, and land surface temperature. Therefore, downscaling thermal imagery can be used to cope with this problem. Several studies have been conducted to downscale satellite imagery (Bechtel, Zakšek, & Hoshayripour, 2012; Bindhu, Narasimhan, & Sudheer, 2013; Dominguez, Kleissl, Luval, & Rickman, 2011; Inamdar & French, 2009). However, some of them produce TIR data with high spatial but low temporal resolution and others generate TIR data with high temporal but usually very coarse spatial resolution. Therefore, development of valuable techniques such as "Spatial and Temporal Adaptive Reflectance Fusion Model (STARFM)" and its derivatives to enhance both spatial and temporal properties of satellite imagery can be of great importance (Amorós-López et al., 2013; Gao, Masek, Schwaller, & Hall, 2006; Gevaert & García-Haro, 2015; Hilker et al., 2009; Zhu, Chen, Gao, Chen, & Masek, 2010). However, these approaches generally used linear models in some parts of their studies. Although linear models have several advantages and have earned their place as the primary tool for process modeling because of their effectiveness and completeness, there are several deficiencies associated with these models (Borel & Gerstl, 1994). Their main drawback is that many real-world phenomena simply do not correspond to the assumptions of a linear model; in these

* Corresponding author.

E-mail address: moosavi_v66@yahoo.com (V. Moosavi).

cases, it is difficult or impossible to produce useful results with linear models. Several robust non-linear methods e.g. artificial intelligence (AI) approaches are developed to cope with these deficiencies. Artificial neural network (ANN) as a robust AI technique organizes an information processing model that stores empirical knowledge through a learning process and subsequently makes the stored knowledge available for future use (Haykin, 1999). It is a powerful computational data model that is able to capture and represent complex input/output relationships. The other robust approach is the combination of fuzzy logic with neural networks i.e. neuro-fuzzy models. In neuro-fuzzy approach, the capability of fuzzy-rules based systems in handling uncertain and complex data and the learning capability of neural networks are combined to produce better predictions. A specific form of neuro-fuzzy systems is the adaptive neuro-fuzzy inference system(ANFIS), which has shown significant results in modeling non-linear functions (Chidthong, Tanaka, & Supharatid, 2009; Jang, Sun, & Mizutani, 1997; Shirmohammadi, Morad, Moosavi, Taie Semiroomi, & Zeinali, 2013). Support vector machine (SVM) as a suitable non-linear, non-parametric modeling technique demonstrates a set of theoretically superior machine-learning algorithms. The development of SVM was initially triggered by the exploration and formalization of learning machine capacity control and over-fitting issues (Vapnik, 1995).

Wavelet transform is a signal processing approach that offers useful decompositions of the original signals, so that wavelet-transformed data enhance the ability of prediction models by capturing useful information on various resolution levels (Adamowski & Sun, 2010; Kisi, 2009; Moosavi, Fallah Shamsi, Moradi & Shirmohammadi, 2013; Moosavi, Vafakhah, Shirmohammadi & Ranjbar, 2013; Nourani, Alami, & Aminfar, 2009). When signal variations are highly non-stationary and the physical processes function under a large range of scales, ANN and ANFIS or SVM models may not be able to cope with non-stationary data if pre-processing of the input and/or output data is not performed (Cannas, Fanni, See, & Sias, 2006).Actually, the wavelets as mathematical functions give a time/position-scale representation of the data and their relationships to analyze data including non-stationarities. Signals are stationary if their properties do not change during the course of the signals. Therefore, non-stationarity can be defined in both spatial and temporal domains. Spatial non-stationarity exists when the same stimulus provokes a different response in different parts of the study region. It is widely recognized that in real applications spatial processes are rarely stationary and isotropic. The wavelet transform has been successfully used in numerous studies in different fields (Borah, Hines, & Bhuyan, 2007; Demirhan & Guler, 2011; Li, 2009; Moosavi & Niazi, 2015; Moosavi, Fallah Shamsi, et al., 2013; Park, Lee, & Song, 2011; Shirmohammadi et al., 2013; Watkins, 2012; Zhou, Bao, Li, Huang, & Yu, 2010).However, to the best of our knowledge, no research has been published that explores coupling wavelet transform with AI models to downscale MODIS LST data. The main objective of this study is to develop a wavelet-artificial intelligence fusion approach (WAIFA) in order to predict daily LST at 100 m-resolution by blending Landsat8 and MODIS data. In fact, this study aims to fill the gaps between two successive Landsat thermal images.

2. Study area and data

The study site located in Tabriz, East Azerbaijan province, Iran, lies between 45°30' to 46°30' E longitudes and 37° to 38° N latitudes (Fig. 1). The average of yearly precipitation and temperature of the study area is 272.3 mm and 13.3 °C, respectively. The climate of the study area is Mediterranean and most of the region's precipitation occurs in just half the year. Landsat 8 images of Path 168, Row 34 acquired in six dates in 2014 from March to August were used as the reference data to estimate daily LST images at 100 m resolution. The corresponding daily MODIS MOD02_QKM, MOD02_HKM, MOD02_1KM and MOD11_L2 data were obtained through the Level 1 and Atmosphere

Archive and Distribution System website data portal available at <http://ladsweb.nascom.nasa.gov/data/search.html>.

3. Methods

3.1. Theoretical basis of the fusion approach

Several fusion algorithms such as spatial and temporal adaptive reflectance fusion model (STARFM) have been developed based on the assumption that MODIS and Landsat surface reflectance are highly consistent (Gao et al., 2006; Weng, Fu, & Gao, 2014). These models assume that there is a linear relationship between the radiances of resampled MODIS data and Landsat data for the homogeneous pixels. Weng et al. (2014) showed that for one pair of Landsat and MODIS image acquired at t_0 , and another MODIS image acquired at t_p , the following relationship can be concluded:

$$R_L(x, y, t_p) = R_L(x, y, t_0) + a \times [R_M(x, y, t_p) - R_M(x, y, t_0)] \quad (1)$$

where R defines the radiance, x and y represents a specific location, t is the acquisition date, L shows Landsat data, M shows MODIS data and a and b are the coefficients for relative adjustment needed for the Landsat and MODIS radiance pixels. Finally, they presented Eq. (2) considering linear spectral un-mixing theory, annual temperature cycle (ATC) and additional information from neighboring pixels.

$$R_L(x_{w/2}, y_{w/2}, t_p) = R_L(x_{w/2}, y_{w/2}, t_0) + \sum_{i=1}^N W_i \times h_i \times [R_M(x_i, y_i, t_p) - R_M(x_i, y_i, t_0)] \quad (2)$$

where W_i is the weight of a neighboring similar pixels, h is the conversion coefficient and N is the number of the spectrally similar pixels.

The WAIFA is based on the relation between the resampled MODIS and Landsat data. One of the main considerations in this modeling approach is that the multi-spectral bands are considered as input data to the modeling process in addition to the TIR data. According to the linear spectral un-mixing approach, pixel response can be approximated by the weighted mean of the pure class responses (end-members) and the area fractions (Verbeiren, Eerens, Piccard, Bauwens, & Van Orshoven, 2007):

$$Y = F \cdot X + e \quad (3)$$

in which, matrix F contains the class area fractions for each pixel, matrix X the pure class responses (end-members), matrix Y contains the mixed image observations and e shows the error. Assuming that end-members in a specific area are fixed (especially in a short period of time), the main variable in calculation of class area fractions is spectral radiances (spectral bands). On the other hand, according to the non-linear spectral un-mixing, MODIS spectral bands and some spectral indices such as the Normalized Difference Vegetation Index (NDVI) can be considered as inputs to predict the fractional areas (Moosavi, Malekinezhad, & Shirmohammadi, 2014). So, the spectral bands are the main predictor variables to calculate land cover fractional areas. Therefore, if spectral bands are imported as input in the modeling process, the sub-pixel changes in the land cover/use and the mixture state in the non-pure pixels are then strictly taken into account. Thus, the Eq. (4) shows the main function of the proposed model:

$$TIR_L(x, y, t_p) = f(TIR_L(x, y, t_0), R_M(x, y, t_p), I_M(x, y, t_p)) \quad (4)$$

where x and y represents a given location, t is the acquisition date, TIR_L is the thermal infrared values for Landsat, R_M shows the spectral and TIR bands of MODIS data and I_M is the spectral indices derived from MODIS data. However, as mentioned before, in the complex systems with severely varying land cover/use, simple regression models

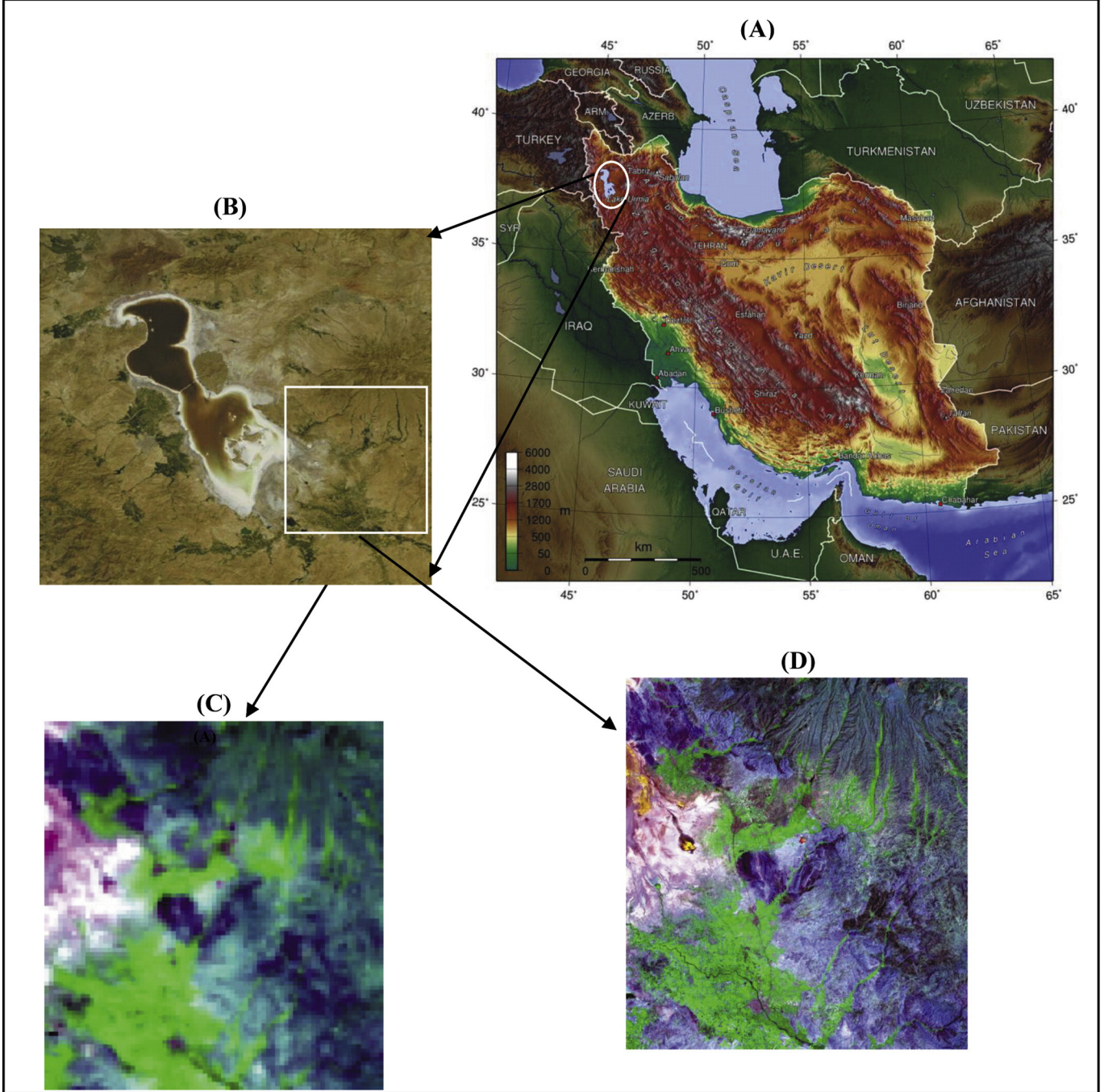


Fig. 1. Study area. A) Location of the study area in Iran, B) An overlook of the study area, C) The MODIS image of the study area, D) The Landsat image of the study area.

may have some deficiencies. Therefore, it is intended in WAIFA that robust AI models to be used to capture the complex relation between low and high resolution data. Toward this purpose, three powerful AI-based modeling approaches i.e. ANN, ANFIS and SVM are tested to select the best one for the presented fusion approach.

Fig. 2 shows the flowchart of the WAIFA model. In the first step, all the images should be registered to the same coordinate system, atmospherically calibrated and corrected to the surface reflectance. Then, the MODIS data are resampled to the size of Landsat 8 TIR data i.e. 100 m using nearest neighbor method. Secondly, all inputs should be decomposed to approximation and detail components using different mother wavelets in different levels. In the next step, the wavelet-based transformed data are imported to the three aforementioned AI models. Then, the developed models are employed to obtain the

predicted Landsat TIR imagery. Statistical criteria such as coefficient of determination and root mean square error can be used to compare the performance of the different model structures. As Yu, Guo, and Wu (2014) showed that the LST inverted from the radiative transfer equation-based method had a good accuracy with RMSE lower than 1 K, the best computed TIR image will be converted to LST using this method Eq. (5).

$$LST = \frac{C_1}{\lambda \ln \left(\frac{C_2}{\lambda^5 \left[\frac{B(T) - I^l - \tau(1-\varepsilon)I^l}{\tau\varepsilon} \right]} + 1 \right)} \quad (5)$$

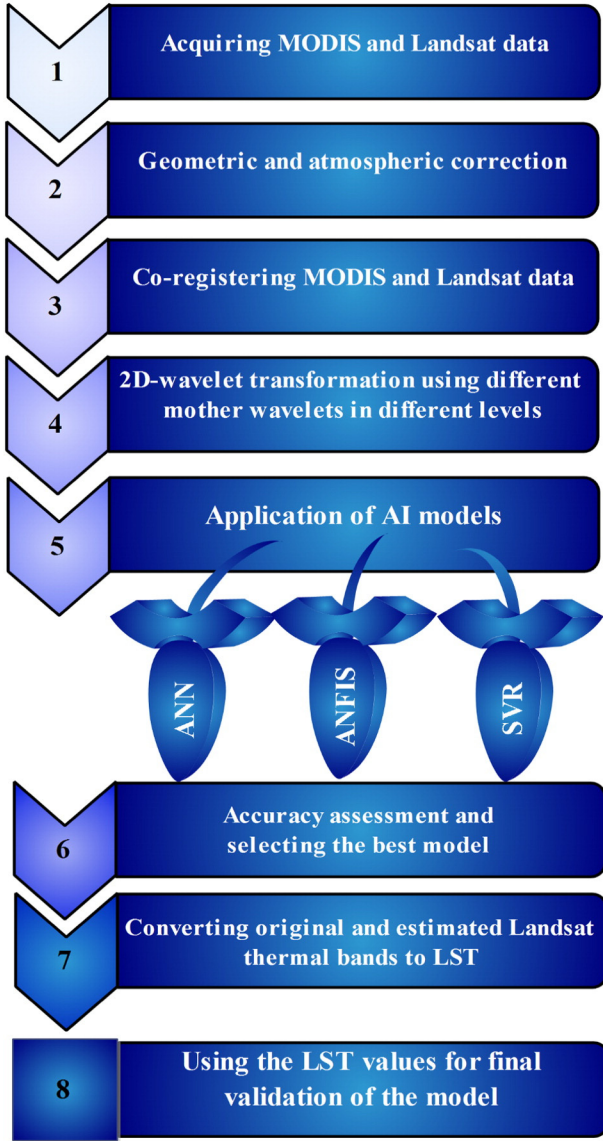


Fig. 2. Flowchart of the study.

where C_1 is $14387.7 \mu\text{m}\cdot\text{K}$, C_2 is $1.19104 \times 10^8 \text{ W }\mu\text{m}^4\cdot\text{m}^{-2}\cdot\text{sr}^{-1}$, λ is the effective band wavelength, $B(T)$ is the radiance received by the sensor with brightness temperature T , I^d is downwelling path radiance, I^u is upwelling path radiance, ε is surface emissivity, and τ is atmospheric transmittance. Below are brief explanations about the AI models used in this approach and the 2D-wavelet transformation.

ANNs are mainly based on a model of imitating the processing of human brain to recognize related spatial and temporal characteristics from the observed data patterns (particularly for non-linear and dynamic evolutions), therefore, they can approximate any level of complexity and do not need prior knowledge of problem solving (Hong, Doll, Revilla, & Nahm, 2011). The Feed-forward back-propagation network as the most commonly used network is a multi-layered neural network, which consists of an input layer, hidden layers, and an output layer. The ANFIS as a universal estimator can approximate any real continuous function on a compact set to any degree of accuracy (Jang et al., 1997). The basic structure of the type of fuzzy inference system can be seen as a model that maps input characteristics to input membership functions. Then, it relates input membership functions to rules and the rules to a set of output characteristics. Finally, it maps output characteristics to output membership functions, and the output membership function to a single output or a decision associated with the output.

Each fuzzy system contains three main parts, fuzzifier, fuzzy database and defuzzifier. Fuzzy database includes two main parts, fuzzy rule base, and inference engine (Jang et al., 1997). Support Vector Regression (SVR) is also a novel learning machine based on the statistical learning theory. In SVR a nonlinear mapping is described to map a training data set, into a high dimensional feature space, in which, there theoretically exists an optimal decision function, to formulate the nonlinear relationship between input data and output data (Vapnik, 1995). The mentioned optimal decision function can be described as:

$$f(x) = w^T \varphi(x) + b \quad (6)$$

where $f(x)$ represents the predicted values; w represents the weights vector and b shows the bias.

The SVR, in fact, focuses on finding the optimum hyper plane and minimizing the structural error:

$$\text{Min } R_c(w, \xi^*, \xi) = \frac{1}{2} w^T w + C \sum_{i=1}^N (\xi_i^* \xi_i), \quad (7)$$

subject to:

$$\begin{aligned} y_i - w^T \varphi(x_i) - b &\leq \varepsilon + \xi_i^*, & i = 1, 2, \dots, N \\ -y_i + w^T \varphi(x_i) + b &\leq \varepsilon + \xi_i, & i = 1, 2, \dots, N \\ \xi_i^* \geq 0 & & i = 1, 2, \dots, N \\ \xi_i \geq 0 & & i = 1, 2, \dots, N \end{aligned}$$

C is a parameter to trade off the first term (which is used to penalize large weights to maintain regression function flatness) and the second term (which decides the balance between confidence risk and experience risk). Training errors above ε are denoted as ξ_i^* whereas training errors below $-\varepsilon$ are denoted as ξ_i . After solving the quadratic optimization problem within equality constraints, and calculating the weights vector, the final SVR regression function is expressed as:

$$f(x) = \sum_{i=1}^N (\beta_i^* \beta_i) K(x_i, x_j) + b \quad (8)$$

where β_i^* and β_i are Lagrangian multipliers, $K(x_i, x_j)$ shows the kernel function, which equals the inner product of two vectors, x_i and x_j , in the feature space $\varphi(x_i)$ and $\varphi(x_j)$, respectively (Ju & Hong, 2013). There are many kinds of kernel function, such as the Gaussian radial basis function (RBF) and polynomial kernel function. More details about SVR and ANN can be found in Haykin (1999).

As the neighboring pixels can affect the prediction of reflectance at a specific date, a 2D wavelet transform can be an effective way to capture the properties of the main signal (original spectral bands) in horizontal, vertical, and diagonal directions. Because of the point based application of AI models they cannot consider the original signal as a single body. In fact, they consider each pixel separately without paying attention to the neighboring pixels. The 2D wavelet transformation can cope with this deficiency of AI models. In fact, wavelet transformation preserves both time and frequency information of the signal. In remote sensing studies,

Table 1

The best structures of ANN, ANFIS and SVM models.

Model	Properties	The best parameter
ANN	Neurons in the hidden layer	12
	Training algorithm	Levenberg–Marquardt
	Iterations	300
ANFIS	Membership function	Bell-shaped (MFgbell)
	Number of membership functions	4
	Iterations	300
SVM	Kernel function	RBF
	Epsilon	0.3
	C	15
	Sigma	5

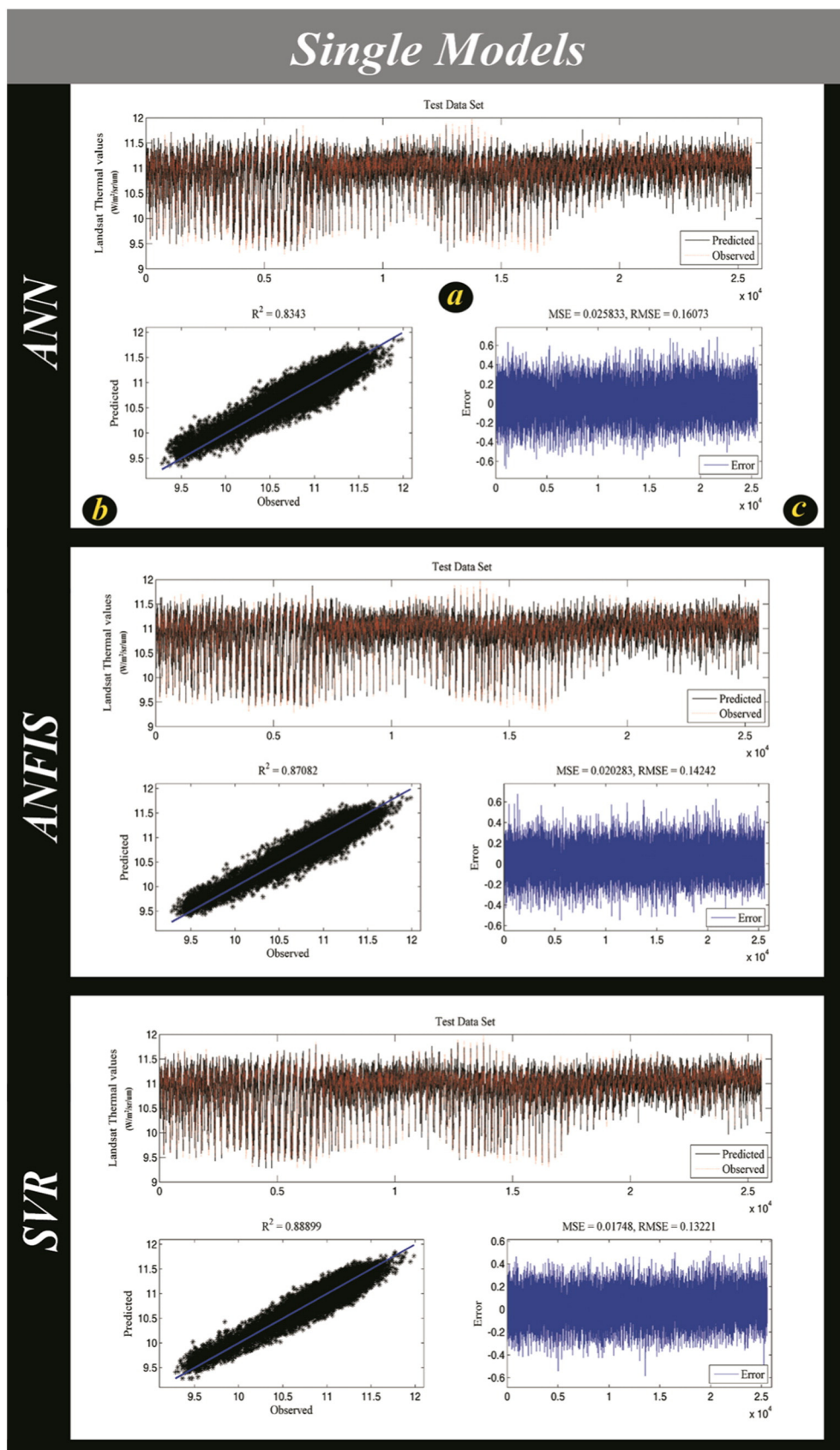


Fig. 3. Best results (test data set) obtained from ANN, ANFIS and SVR in their single form.

the time domain can be substituted by other domains such as position of the pixels. The wavelet transform breaks the signal into its wavelets (small wave) which are scaled and shifted versions of the original wavelet (mother wavelet). The wavelet transformation is of two kinds including continuous wavelet transformation (CWT) and discrete wavelet transformation (DWT). The CWT computation requires a large quantity of calculation time and resources. The discrete wavelet transform (DWT) necessitates less calculation time. DWT scales and positions are usually based on powers of two (dyadic scales and positions). The discrete wavelet transformation (DWT) can be introduced as:

$$\Psi_{j,k}(t) = \frac{1}{\sqrt{|s_0^j|}} \Psi\left(\frac{t-k\tau_0 s_0^j}{s_0^j}\right) \quad (9)$$

where j and k are integers and s_0 which is greater than zero is a fixed dilation step (Cannas et al., 2006). The DWT performs two sets of functions namely high-pass and low-pass filters. The outputs of the low-pass filter are the approximation coefficients and the outputs of the high-pass filter are the detail coefficients. The decomposition is repeated to further increase the frequency resolution and the approximation coefficients decomposed with high and low pass filters and then down-sampled. This is represented as a binary tree which is known as a filter bank.

A two-dimensional wavelet decomposition can be described as a one-dimensional discrete wavelet transform applied consecutively along the horizontal, vertical and diagonal directions (Mallat, 1989). In fact, in the two dimensional wavelet transform, one dimensional decompositions are performed in different directions. It produces Vertical, Horizontal and Diagonal components. In the horizontal component, the wavelet transform is applied to the rows of the imagery, in the vertical component, the wavelet transform is applied to the columns of the imagery and finally, in the diagonal component, the wavelet transform is performed on the diagonal direction. In this way, the properties of the main image are assessed in different directions. Therefore, the neighboring pixels are fully considered. Another choice is to perform one dimensional wavelet transform if the 2D transform does not produce satisfactory results. In this process (for one-dimensional decomposition), all 2D input signals are first reshaped to a one dimensional signal, the 1D transform is applied to the reshaped signals.

3.2. Model implementation

As the first step in application of WIAFA, both MODIS and Landsat data were registered to the same coordinate system and resampled to the same spatial resolution (100 m). The MOD02_QKM, MOD02_HKM,

and MOD02_1KM datasets were used as inputs for the models and also for visual interpretation to help accurate co-registration between two sets of data.

In co-registering process, each MODIS pixel was replicated into 10, 100-m pixels to match the Landsat 8 spatial resolution. Then, the high-resolution image was considered as the reference image and the low-resolution image was registered to the high-resolution image using well-distributed GCPs and a 1st order polynomial transformation. Then, a common geographical area was determined and extracted from the images, which covered the study area. In the next step, the co-registered imageries were overlaid over one another to examine potential pixel misalignment caused by the different spatial resolutions between MODIS and Landsat images. The misalignment was then corrected by offsetting the MODIS image based on the coordinates of the upper-left corner of the Landsat 8 image (Stathopoulou & Cartalis, 2009). All satellite images were atmospherically corrected using the Chavez (1996) model. The Digital Numbers (DNs) were converted back to top of atmosphere (TOA) spectral radiance through radiometric calibration process using sensor calibration function (Chander & Markham, 2003; Melesse, 2004). Radiance values were then converted into surface reflectance using the Eq. (10).

$$\rho = \frac{(L_{TOA} - L_p)\pi d^2}{ESUN_\lambda \cos\theta_z T_z} x \quad (10)$$

where, ρ is surface reflectance, L_{TOA} is spectral radiance, L_p is radiance resulted from the interaction of aerosol and atmospheric particles, d is earth-sun distance(in Astronomical Units), $ESUN_\lambda$ is band pass solar irradiance at TOA, θ_z is solar zenith angle (in degree) and T_z is atmospheric transmissivity between ground and TOA. In this study, the cloud cover were first masked and cloud-free images were then imported to the modeling process. It should be noted that each cloud pixel of a MODIS image can be replaced with its corresponding pixels in another MODIS image that is not covered by cloud. However, as the proposed method was aimed to be performed on the original images without any change, cloud cover were masked in the first step.

After preprocessing satellite imagery, the spectral indices such as NDVI and EVI were produced using resampled MODIS data. Therefore, input data included spectral reflectance of 7 MODIS bands (Moosavi et al., 2014), MODIS TIR bands, Normalized Difference Vegetation Index (NDVI), Enhanced Vegetation Index (EVI), Landsat TIR band for time t_0 , and the output data is the Landsat TIR band for time t_p .

In order to wavelet based transform the original input signals, different kinds of mother wavelets were used to decompose the original data in different levels i.e. 1, 2, 3, 4 and 5 levels. The mother wavelets were selected according to the literature review. In this study, "Haar" wavelet as a simple wavelet, Daubechies (db) wavelet as the most popular

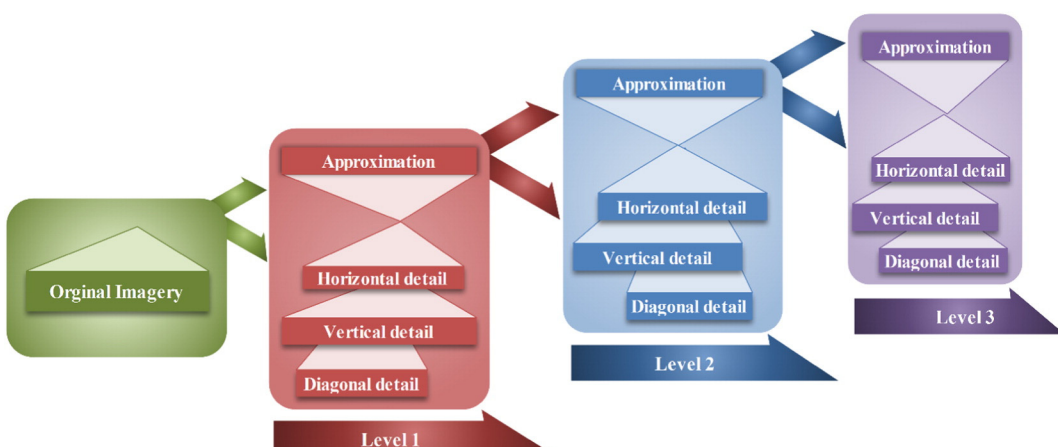


Fig. 4. Schematic demonstration of the wavelet based decomposition process in different levels.

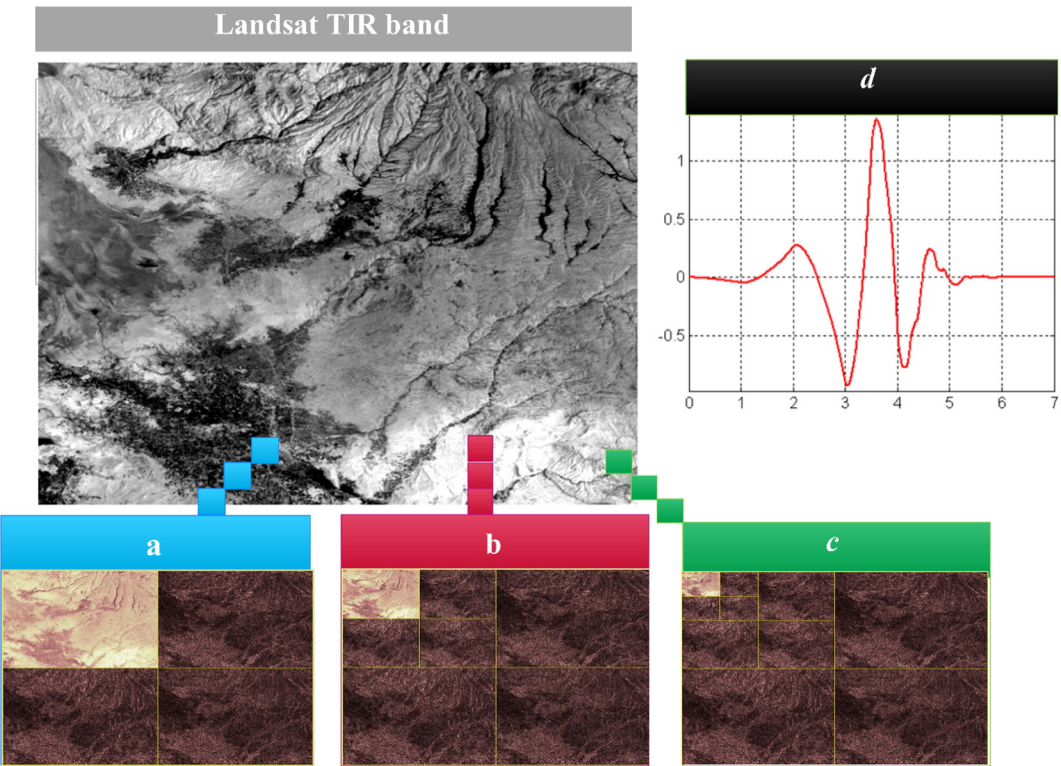


Fig. 5. An example of decomposed Landsat thermal band using “db4” mother wavelet in levels a) 1, b) 2 and c) 3. Part d is a schematic presentation of db4 mother wavelet.

wavelet (Mallat, 1989), and some other wavelets such as sym, bior, rboi and coif were used in the transformation process. In the 2D wavelet transform, the one dimensional wavelet analysis is first applied to the columns of the image and then applied to the rows and diagonal direction. Therefore, in each decomposition level there are one “Approximate” component and three “Detail” components called vertical,

horizontal and diagonal detail components. The decomposed data then were imported to the ANN, ANFIS and SVR models.

Feed-forward neural network (FNN) as a popular ANN algorithm (Haykin, 1999) was used in this study. Tuning the network parameters is one of the most important parts in the ANN modeling process. In order to select the best network structure, different numbers of nodes

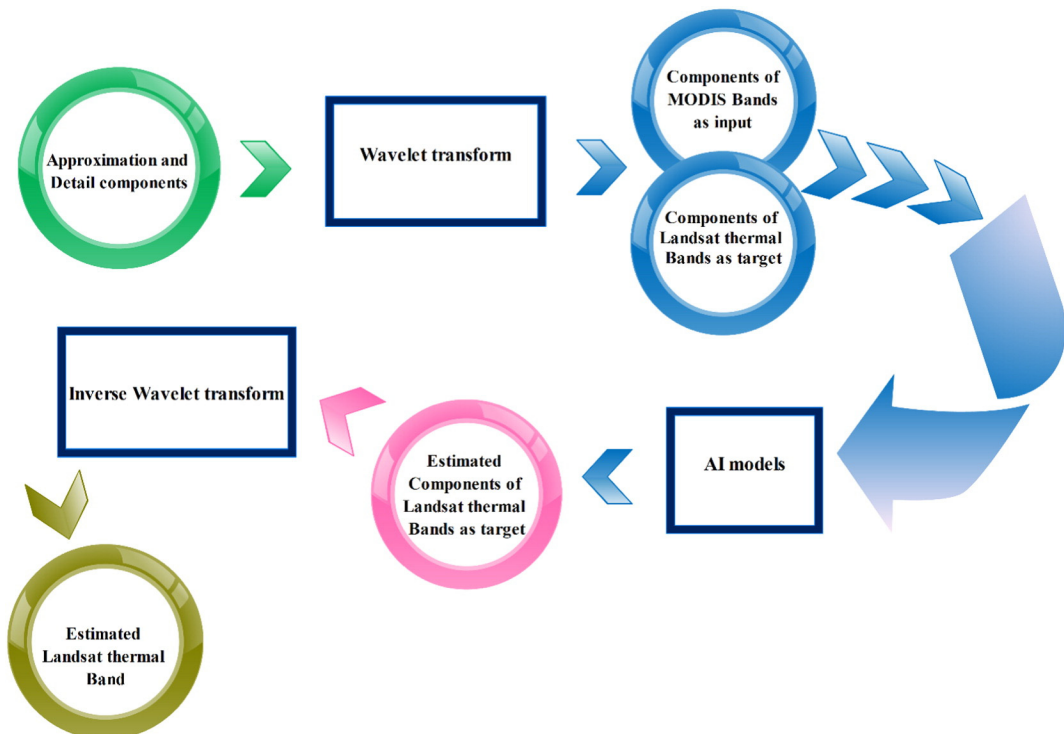


Fig. 6. Steps of wavelet-based modeling procedure.

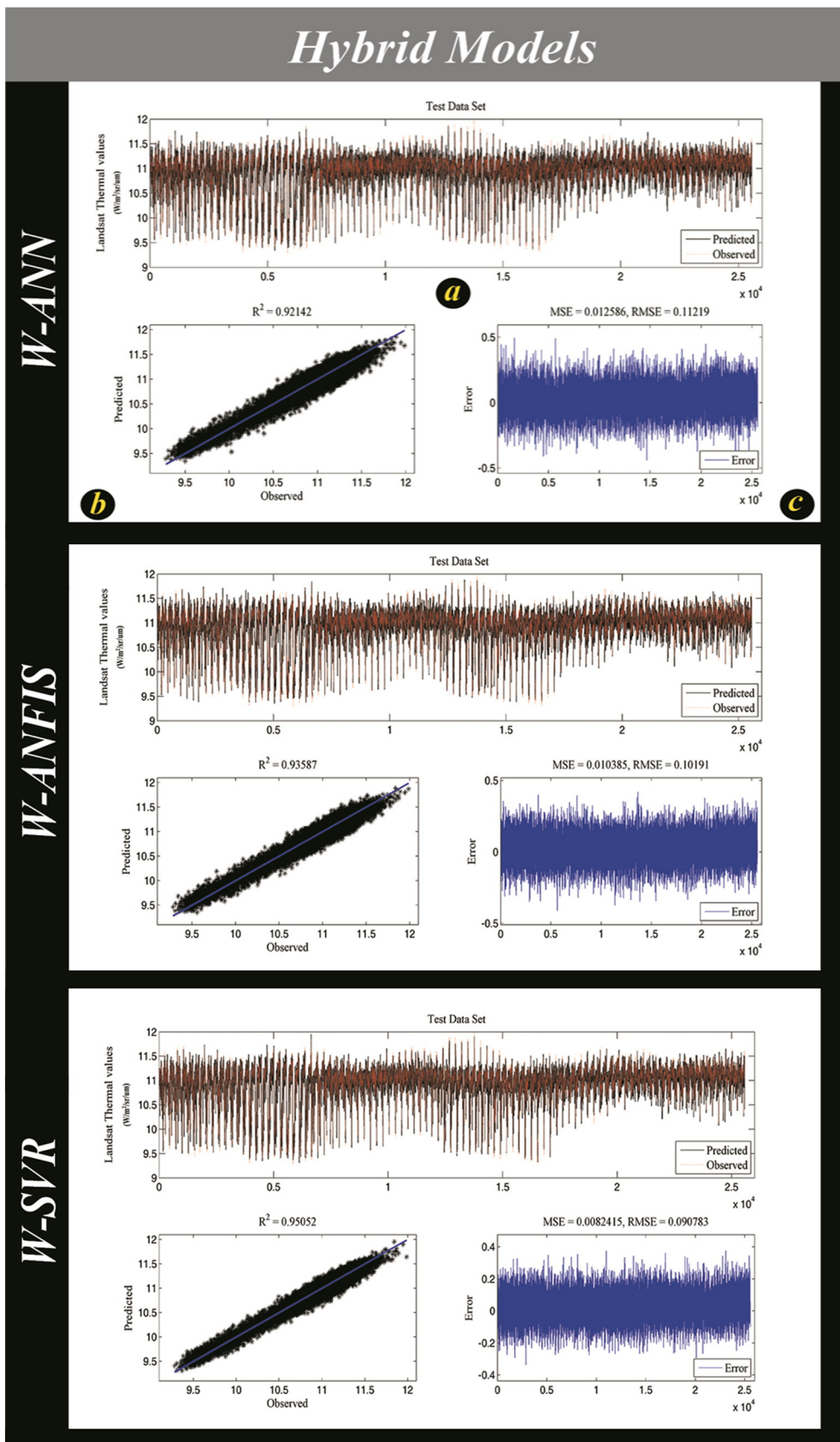


Fig. 7. Best results (test data set) obtained from W-ANN, W-ANFIS and W-SVR.

Table 2

The performance of the proposed model (W-SVR) to produce LST data in different dates.

Date	Landsat overpass Time	MODIS overpass time	R ²	Mean error (K)	Mean absolute error (K)	R ² (for linear regression)
03/07/2014	12:02	12:15	0.914	0.87	1.49	0.54
04/07/2014	12:02	12:15	0.903	1.01	1.93	0.54
05/26/2014	12:02	12:15	0.928	0.74	1.07	0.56
07/13/2014	12:02	12:15	0.945	-0.47	0.98	0.59
07/29/2014	12:02	12:15	0.950	0.39	0.85	0.61
08/14/2014	12:02	12:15	0.952	0.17	0.47	0.62

were tested in the hidden layer. The number of nodes was selected using a common trial-and-error approach. Different transfer functions such as tangent hyperbolic and tangent sigmoid were also tested for the hidden and output layers. 70 percent of the data were used for training and 30 percent for testing in the network performance. Three different algorithms were used in order to train the networks. The first training algorithm was Gradient descent with momentum and adaptive learning rate back-propagation (GDX) which uses back-propagation to calculate derivatives of performance cost function with respect to the weight and bias variables of the network. The second training algorithm was Levenberg–Marquardt (LM) which is a modification of the classic Newton algorithm for finding an optimum solution to a minimization problem (Maier & Dandy, 1998). The last training algorithm was Bayesian regularization (BR) which is an algorithm that automatically sets optimum values for the parameters of the objective function. In the approach used, the weights and biases of the network are assumed to be random variables with specified distributions. In the ANFIS model, three parameters should be set i.e. membership functions (MF) type,

number of membership functions and number of iterations. Toward this purpose four different popular MFs namely Gaussian (MFgauss), bell-shaped (MFbell), triangular (MFtri), and spline-based (MFPi), or Piduetots shape have been used. ANFIS models with different types of MF have been run with 2, 3, 4, and 5 MFs and with 100, 300, 500, 1000 and 1500 iterations for each node of input data.

SVR uses an implicit feature space mapping from the dimension of the data to a probably infinite feature space, using a non-linear demonstration of the modeled data; this is done through the ‘kernel trick’ (Smola & Schlkopf, 2004). As mentioned before, type of kernel functions is one of the most important parameters that should be set in SVR modeling. In this study, two popular kernels with wide applicability within SVR namely Radial Basis Function (RBF) and polynomial were used (Crone, Lessmann, & Pietsch, 2006). The best value for kernel width parameter (σ) has to be selected. A large value of σ causes similarity in input patterns and lead to under-fitting of the function. On the other hand, too small value of σ , causes dissimilarity and subsequently over-fitting of the function (Chang, Chen, & Wang, 2005). The factor, C, which controls the trade-off between training error and model complexity is the other important parameter that should be accurately set (Basak, Pal, & Patranabis, 2007). A large amount of C will overfit the data while small C means that the model does not fit the learning data (Lendasse, Ji, Reyhani, & Verleysen, 2005).

4. Results and discussion

After radiometric calibration, geometric rectification, atmospheric correction and co-registering MODIS and Landsat data, the AI-based modeling approaches were performed. Table 1 shows the best structures of ANN, ANFIS and SVM models. Fig. 3 shows the best results (test dataset) obtained from ANN, ANFIS and SVR in their single form

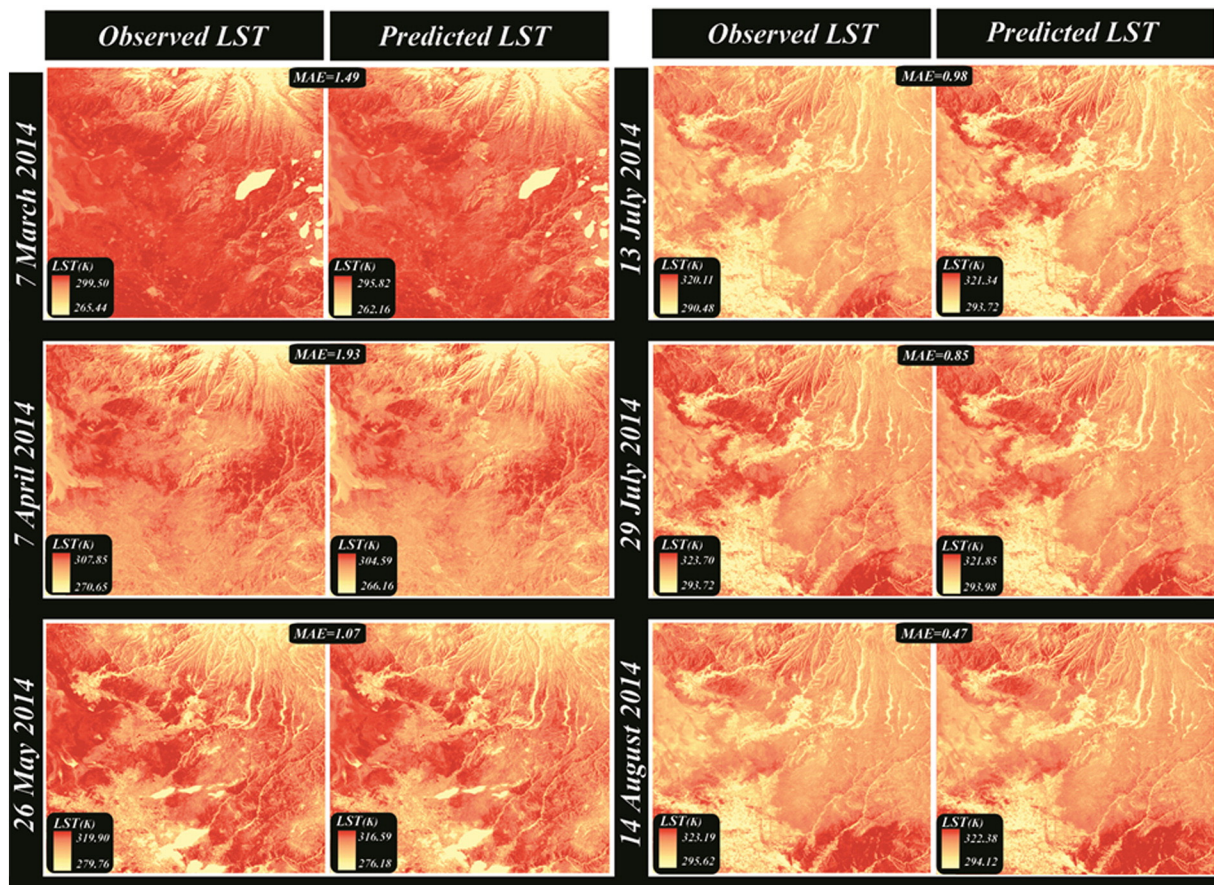


Fig. 8. Observed (original) and predicted Landsat LSTs using the W-SVR model (as the best model). MAE is Mean Absolute Error.

for date 14th August 2014 (as an example). Part "a" compares the observed and estimated thermal values, part "b" shows the scatter plot between observed and estimated thermal values, and part "c" shows the variations of error. SVR is the best single model with an R^2 of 0.89 and an RMSE of 0.13. ANFIS ranked second with the R^2 of 0.87 and the RMSE of 0.14. However, ANN has the least coefficient of determination (0.83) and the largest RMSE (0.16). As it is obvious from these figure, ANFIS outperformed ANN. This may be related to the effect of fuzzification of the input through membership functions. Because the data were first fuzzified and then these data have been imported to the ANN model and neural network modeling have been performed on the fuzzified data, the ability of this modeling approach have been improved (Moosavi, Vafakhah, Shirmohammadi & Behnia, 2013). The superior performance of SVR may be related to its ability to solve the convex optimization problems in which all local solutions are classified into a global optimum (Bishop, 1994). SVR does not consider any assumption about the functional form of the transformation because the kernel implicitly contains a nonlinear transformation. Also, SVRs provide a good out-of-sample generalization, if the parameters are appropriately chosen. This means that, even if the training sample has some bias, choosing proper parameters, SVRs perform appropriately. SVRs provide a unique solution, since the optimality problem is convex. This is an advantage in comparison to the neural networks, which have multiple solutions related to local minima and therefore they may not be robust over different samples. The other advantage of SVR is that it minimizes the structural risk rather than minimizing the error which is performed in ANN and ANFIS models. SVRs also gain flexibility in their modeling using the Kernel tricks. It needs not be linear and even needs not have the same functional form for all data, since its function is non-parametric and operates locally. Totally, all of the aforementioned models can be used to estimate Landsat thermal band with a coefficient of determination of more than 0.8 which can be acceptable regarding to the easiness and feasibility of these models.

In order to develop hybrid models, the original bands were first decomposed using different mother wavelets in different levels. Schematic demonstration of the wavelet based decomposition process in different levels can be shown as Fig. 4. As it is shown in this figure, in the first level, the original image is decomposed to one approximation and three detail images. The 2-D wavelet transform is usually performed by applying filters to the image. Typically, Low and High-pass filters are used. The convolution with the low-pass filter results in a so-called approximation image and the convolutions with the High-pass filter in specific directions result in so-called detail images. The approximation is then split itself into a second level of approximation and details. And this process is performed iteratively. In fact, the low frequency components (approximations) can be further decomposed until the desired resolution is reached. When multiple levels of decomposition are applied, the process is referred to as multi-resolution decomposition.

Fig. 5 shows a decomposed Landsat thermal band using "db4" mother wavelet in levels 1, 2 and 3, as an example. Part 'a' shows the decomposition in level 1. In this decomposition, 3 images are produced i.e. one approximation and three details. In part 'b' the approximation produced in previous level, is decomposed to one approximation and 3 details. The same procedure is done in part 'c'. The produced components of MODIS and Landsat bands then were imported to the mentioned AI models as inputs and targets. After performing the modeling process, and estimating the decomposed Landsat thermal band, the inverse 2-D wavelet transformation was applied to obtain the final predicted Landsat thermal band. Fig. 6 shows the steps of this procedure.

The mother wavelet "db4" was the best mother wavelet and level 2 was the best decomposition level in all hybrid models. Fig. 7 shows the best results (test data set) obtained from hybrid models i.e. W-ANN, W-ANFIS and W-SVR. It is confirmed that the hybrid wavelet based AI approaches outperformed the single AI approaches. As for the single models, the performance of hybrid approaches is in the following order: W-SVR, W-ANFIS and W-ANN. Hybrid W-SVR model produced

the best results with R^2 of 0.9505 and RMSE of 0.09. W-ANFIS with an R^2 of 0.9358 and an RMSE of 0.10 was the second model. W-ANN has the least correlation coefficient (0.9214) and the largest RMSE (0.11) among hybrid models. This study shows that 2D-wavelet transform can effectively enhance the ability of AI techniques for blending Landsat and MODIS thermal bands by decomposing the original data into several sub-bands. In fact, wavelet transformation extracted details and provide more detailed components to be imported to the AI models. The wavelet transform is of specific attention for analysis of non-stationary and fast transient signals. Signals are stationary if their properties do not change during the course of signals. Two-dimensional images are non-stationary because the edges, textures, and deterministic objects are distributed at different locations and orientations. Wavelet transforms isolate frequencies in both time and space, allowing detail information to be easily extracted from satellite imagery (Paul & Ramamoorthy, 2013). Therefore, they can help AI models to capture the properties of non-stationary signals. Finally, it can be determined that hybrid W-AI models are good tools for downscaling MODIS thermal bands. Therefore, the Wavelet-SVR can be introduced as the final hybrid model for blending Landsat and MODIS data.

As a final step, the observed and estimated Landsat thermal bands (using the proposed Wavelet-SVR model) were converted to the land surface temperature using Split-Window (SW) algorithm. This was performed in order to determine the performance of developed models to produce LST data as an additional validation. Table 2 shows the performance of the proposed model (W-SVR) to produce LST data(100 m LST imagery) in different dates. The R^2 values for the linear regression is also added for comparison. The mean absolute difference between observed and estimated LST ranged from 0.47 K to 1.93 K. This shows that the proposed model can satisfactorily downscale MODIS land surface temperature to the resolution of Landsat thermal bands.

Fig. 8 shows the observed (original) and predicted Landsat LSTs. It is understandable from these figures that there is a good consistency between observed (original) and predicted imagery in all dates. Weng et al. (2014) stated that if land covers or other surface conditions did change, it could lead to some errors in the prediction. Therefore, the time period of the study should be divided to parts with minimum change in the surface conditions. Therefore, the training of the model can be performed for example for each month or each season, separately. The proposed model can appropriately determine the relation between MODIS and Landsat data using non-linear artificial intelligence models. The other merit of the proposed model is the use of a powerful signal processing approach i.e. 2D-wavelet transform which is able to capture the properties of Landsat and MODIS data in different directions. Therefore, different changes and patterns especially between neighboring pixels can be strictly detected and considered in the AI-based modeling process. So, an important advantage of the proposed model is that it can fairly detect the non-linearity and non-stationarity in the satellite imagery. As mentioned before, WIAFA is proposed to fill the gaps between two successive Landsat images. As the temporal resolution of Landsat images is 16 days, it is suggested that each Landsat image be used as input to estimate Landsat thermal values in its 8 previous days and its 8 next days. Therefore, the maximum difference between each base image (imagery in time t_0) and the target image (imagery in time t_p) is 8 days. It can improve the performance of the proposed model by reducing the effect of the surface condition changes.

5. Conclusion

This research proposed wavelet-artificial intelligence fusion approach (WAIFA), to estimate land surface temperature at high temporal frequency (daily) and at the medium spatial resolution (100 m). In this study, MODIS and Landsat 8 datasets were used. The WAIFA algorithm, combines a powerful signal processing method i.e. wavelet transformation with Artificial Intelligence approaches to produce a hybrid model which is fairly able to blend MODIS and Landsat 8 datasets. This paper

has examined in details the theoretical basis and the implementation procedures of WAIFA. An experiment was also performed to predict LSTs of six dates in 2014 from March to August. This approach presented several enhancements over previous models. One of the main improvements was to use a non-linear modeling scheme which can cope with the non-linear nature of the land surface temperature data. The other advantage of this approach is to use multi-spectral bands and different spectral indices in addition to thermal data in the modeling process. This can help the model to consider the mixture properties of MODIS pixels. In fact, sub-pixel changes in the land cover/use and the mixture state in the non-pure pixels is strictly taken into account by importing spectral bands the modeling process. Using a 2D wavelet transform the properties of the main signals (original bands) were captured in horizontal, vertical, and diagonal directions to consider the effect of neighboring pixels and to cope with the non-stationary properties of the satellite and land surface temperature data. Some considerations should be taken in applying this approach. Several parameters must be judiciously tuned in AI models, e.g., number of neurons in the hidden layer and training function in the ANN model, number and type of membership functions in ANFIS model and epsilon, C and Sigma in SVR model. In the wavelet transforms also, the mother wavelet and the decomposition level should be carefully set. Application of this model to other sensors, such as ASTER, to enhance their temporal resolution, improvement of the fusion model to resolve the cloud contamination issue (instead of masking cloudy areas), using principle component analysis as a further pre-processing approach on the original bands and application of other AI models such as self-organizing map (SOM), Hopfield Networks and radial basis functions (RBF) can be suggested as future works.

References

- Abuzar, M., O'Leary, G., & Fitzgerald, G. (2009). Measuring water stress in a wheat crop on a spatial scale using airborne thermal and multispectral imagery. *Field Crops Research*, *112*, 55–65.
- Adamowski, J., & Sun, K. (2010). Development of a coupled wavelet transform and neural network method for flow forecasting of non-perennial rivers in semi-arid watersheds. *Journal of Hydrology*, *390*(1–2), 85–91.
- Agam, N., Kustas, W.P., Anderson, M.C., Li, F., & Neale, C.M.U. (2007). A vegetation index based technique for spatial sharpening of thermal imagery. *Remote Sensing of Environment*, *107*, 545–558.
- Amorós-López, J., Gómez-Chova, L., Alonso, L., Guanter, L., Zurita-Milla, R., & Moreno, J. (2013). Multitemporal fusion of Landsat/TM and ENVISAT/MERIS for crop monitoring. *International Journal of Applied Earth Observation and Geoinformation*, *23*, 132–141. <http://dx.doi.org/10.1016/j.jag.2012.12.004>.
- Anderson, M.C., Norman, J.M., Kustas, W.P., Houborg, J., Starks, P.J., & Agam, N. (2008). A thermal-based remote sensing technique for routine mapping of land-surface carbon, water and energy fluxes from field to regional scales. *Remote Sensing of Environment*, *112*, 4227–4241.
- Anderson, M.C., Allen, R.G., Morse, A., & Kustas, W.P. (2012). Use of Landsat thermal imagery in monitoring evapotranspiration and managing water resources. *Remote Sensing of Environment*, *112*, 50–65.
- Badeck, F.W., Bondeau, A., Bottcher, K., Doktor, D., Lucht, W., Schaber, J., & Sitch, S. (2004). Responses of spring phenology to climate change. *The New Phytologist*, *162*, 295–309.
- Basak, D., Pal, S., & Patranabis, D.C. (2007). Support vector regression. *Neural Information Processing - Letters & Reviews*, *11*(10), 203–224.
- Bechtel, B., Záskýk, K., & Hoshyaripour, G. (2012). Downscaling land surface temperature in an urban area: a case study for Hamburg, Germany. *Remote Sensing*, *4*(10), 3184–3200.
- Bindhu, V.M., Narasimhan, B., & Sudheer, K.P. (2013). Development and verification of a non-linear disaggregation method (NL-DisTrad) to downscale MODIS land surface temperature to the spatial scale of Landsat thermal data to estimate evapotranspiration. *Remote Sensing of Environment*, *135*, 118–129.
- Bishop, C.M. (1994). Novelty detection and neural network validation. *Proceedings of the IEEE Conference on Vision, Image and Signal Processing* (pp. 217–222).
- Borah, S., Hines, E.L., & Bhuyan, M. (2007). Wavelet transform based image texture analysis for size estimation applied to the sorting of tea granules. *Journal of Food Engineering*, *79*, 629–639.
- Borel, C.C., & Gerstl, S.A. (1994). Nonlinear spectral mixing models for vegetative and soil surfaces. *Remote Sensing of Environment*, *47*, 403–416.
- Cannas, B., Fanni, A., See, L., & Sias, G. (2006). Data preprocessing for river flow forecasting using neural networks: wavelet transforms and data partitioning. *Physics and Chemistry of the Earth*, *31*, 1164–1167.
- Chander, G., & Markham, B. (2003). Revised landsat-5 TM radiometric calibration procedures and post calibration dynamic ranges. *IEEE Transactions on Geoscience and Remote Sensing*, *41*, 2674–2677.
- Chang, Q., Chen, Q., & Wang, X. (2005). Scaling Gaussian RBF kernel width to improve SVM classification. *International Conference on Neural Networks and Brain, ICNN and B'05 Beijing*.
- Chavez, P.S., Jr. (1996). Image-based atmospheric corrections-revisited and improved. *Photogrammetric Engineering and Remote Sensing*, *62*, 1025–1036.
- Chidthong, Y., Tanaka, H., & Supharatid, S. (2009). Developing a hybrid multi-model for peak flood forecasting. *Hydrological Processes*, *23*(12), 1725–1738.
- Crone, S.F., Lessmann, S., & Pietsch, S. (2006). Parameter sensitivity of support vector regression and neural networks for forecasting. *Proceedings of the 2006 International Conference on Data Mining Las Vegas*.
- Demirhan, A., & Guler, I. (2011). Combining stationary wavelet transform and self-organizing maps for brain MR image segmentation. *Engineering Applications of Artificial Intelligence*, *24*, 358–367.
- Dominguez, A., Kleissl, J., Luvall, J.C., & Rickman, D.L. (2011). High-resolution urban thermal sharpener (HUTS). *Remote Sensing of Environment*, *115*, 1772–1780.
- Dragutin, T.M., & Eitzinger, J. (2007). Modelling temperatures of crop environment. *Ecological Modelling*, *202*, 465–475.
- Gao, F., Masek, J., Schwaller, M., & Hall, F. (2006). On the blending of the Landsat and MODIS surface reflectance: predicting daily Landsat surface reflectance. *IEEE Transactions on Geoscience and Remote Sensing*, *44*(8), 2207–2218.
- Gevaert, C.M., & García-Haro, F.J. (2015). A comparison of STARFM and an unmixing-based algorithm for Landsat and MODIS data fusion. *Remote Sensing of Environment*, *156*, 34–44.
- Griendveld, A.A., & Owe, M. (1993). On the relationship between thermal emissivity and the normalized difference vegetation index for natural surfaces. *International Journal of Remote Sensing*, *14*, 1119–1131.
- Haykin, S. (1999). *Neural networks: a comprehensive foundation* (2nd ed.). Upper Saddle River, New Jersey: Prentice Hall.
- Hilker, T., Wulder, M.A., Coops, N.C., Linke, J., McDermid, G., Masek, J.G., et al. (2009). A new data fusion model for high spatial- and temporal-resolution mapping of forest disturbance based on Landsat and MODIS. *Remote Sensing of Environment*, *113*(8), 1613–1627.
- Hong, P., Doll, W.J., Revilla, E., & Nahm, A.Y. (2011). Knowledge sharing and strategic fit in integrated product development projects: an empirical study. *International Journal of Production Economics*, *132*, 186–196.
- Hulley, G.C., Hook, S.J., & Baldridge, A.M. (2010). Investigating the effects of soil moisture on thermal infrared land surface temperature and emissivity using satellite retrievals and laboratory measurements. *Remote Sensing of Environment*, *114*, 1480–1493.
- Ichoku, C., Kaufman, Y.J., Giglio, L., Li, Z., Fraser, R.H., Jin, J.Z., & Park, W.M. (2003). Comparative analysis of daytime fire detection algorithms using AVHRR data for the 1995 fire season in Canada: perspective for MODIS. *International Journal of Remote Sensing*, *24*, 1669–1690.
- Inamdar, A.K., & French, A. (2009). Disaggregation of GOES land surface temperatures using surface emissivity. *Geophysical Research Letters*, *36*.
- Jang, J.S.R., Sun, C.T., & Mizutani, E. (1997). *Neuro-fuzzy and soft computing: a computational approach to learning and machine intelligence*. Upper Saddle River: Prentice-Hall.
- Jeganathan, C., Hamm, N.A.S., Mukherjee, S., Atkinson, P.M., Raju, P.L.N., & Dadhwal, V.K. (2011). Evaluating a thermal image sharpening model over a mixed agricultural landscape in India. *International Journal of Applied Earth Observation and Geoinformation*, *13*, 178–191.
- Ju, F.Y., & Hong, W.C. (2013). Application of seasonal SVR with chaotic gravitational search algorithm in electricity forecasting. *Applied Mathematical Modelling*, *37*, 9643–9651.
- Karnieli, A., Bayasgalan, M., Bayarjargal, Y., Agam, N., Khudulmur, S., & Tucker, C.J. (2006). Comments on the use of the vegetation health index over Mongolia. *International Journal of Remote Sensing*, *27*, 2017–2024.
- Karnieli, A., Agam, N., Pinker, R.T., Anderson, M., Imhoff, M.L., Gutman, G.G., ... Goldberg, A. (2010). Use of NDVI and land surface temperature for drought assessment: merits and limitations. *Journal of Climate*, *23*, 618–633.
- Kisi, O. (2009). Neural networks and wavelet conjunction model for intermittent stream flow forecasting. *Journal of Hydrologic Engineering*, *14*, 773–782.
- Lendasse, A., Ji, Y., Reyhani, N., & Verleysen, M. (2005). LS-SVM hyper parameter selection with a nonparametric noise estimator. Part II. In W. Duch, J. Kacprzyk, E. Oja, & S. Zadrożny (Eds.), *Proceedings of the 15th International Conference, Warsaw, Poland, September 11–15, 2005*.
- Li, T.S. (2009). Applying wavelet transform, rough set theory and support vector machine for copper clad laminate defects classification. *Expert Systems with Applications*, *36*(3), 5822–5829.
- Maier, H.R., & Dandy, G.C. (1998). Understanding the behavior and optimizing the performance of back-propagation neural networks: an empirical study. *Environmental Modelling and Software*, *13*, 179–191.
- Mallat, S.G. (1989). A theory for multi resolution signal decomposition: the wavelet representation. *IEEE Transactions on Pattern Analysis and Machine Intelligence*, *11*, 674–693.
- Melesse, A.M. (2004). Spatiotemporal dynamics of land surface parameters in the Red River of North Basin. *Physics and Chemistry of the Earth, Parts A/B/C*, *29*, 795–810.
- Moosavi, V., & Niazi, Y. (2015). Development of hybrid wavelet packet-statistical models (WP-SM) for landslide susceptibility mapping. *Landslides* <http://dx.doi.org/10.1007/s10346-014-0547-0>.
- Moosavi, V., Vafakhah, M., Shirmohammadi, B., & Ranjbar, M. (2013a). Optimization of wavelet-ANFIS and wavelet-ANN hybrid models by Taguchi method for groundwater level forecasting. *Arabian Journal for Science and Engineering*, *39*, 1785–1796.
- Moosavi, V., Fallah Shamsi, S.R., Moradi, H.R., & Shirmohammadi, B. (2013b). Application of Taguchi method to satellite image fusion for object-oriented mapping of Barchan dunes. *Geosciences Journal* <http://dx.doi.org/10.1007/s12303-013-0044-9>.

- Moosavi, V., Vafakhah, M., Shirmohammadi, B., & Behnia, N. (2013c). A wavelet-ANFIS hybrid model for groundwater level forecasting for different prediction periods. *Water Resources Management*, 27, 1301–1321.
- Moosavi, V., Malekinezhad, H., & Shirmohammadi, B. (2014). Fractional snow cover mapping from MODIS data using wavelet-artificial intelligence hybrid models. *Journal of Hydrology*, 511, 160–170.
- Muramatsu, K., Nakayama, S., & Kaihatsu, I. (2006). A case study of estimating thermal energy budget in Mongolian plateau using LANDSAT 7/ETM + data. *Advances in Space Research*, 38, 2191–2195.
- Nourani, V., Alami, M.T., & Aminfar, M.H. (2009). A combined neural-wavelet model for prediction of watershed precipitation, Lighvanchai, Iran. *Engineering Applications of Artificial Intelligence*, 16, 1–12.
- Park, C.J., Lee, H.K., & Song, W.Y. (2011). Thorsten Graeve Achterkirchen, Ho Kyung Kim, 2011, defective pixel map creation based on wavelet analysis in digital radiography detectors. *Nuclear Instruments and Methods A*, 634, 101–105.
- Paul, L., & Ramamoorthy, P. (2013). Synthetic aperture radar image change detection using fuzzy c-means clustering algorithm. *IJARCSEE*, 2(3), 1374–1379.
- Rojas, O., Vrielink, A., & Rembold, F. (2011). Assessing drought probability for agricultural areas in Africa with coarse resolution remote sensing imagery. *Remote Sensing of Environment*, 115, 343–352.
- Shirmohammadi, B., Morad, H.R., Moosavi, V., Taie Semiroomi, M., & Zeinali, A. (2013). Forecasting of meteorological drought using Wavelet- ANFIS hybrid model for different time steps (case study: southeastern part of east Azerbaijan province, Iran). *Natural Hazards*, 69, 389–402.
- Smola, A.J., & Schlkopf, B. (2004). A tutorial on support vector regression. *Statistics and Computing*, 14(3), 199–222.
- Sobrino, J.A., Gomez, M., Munoz, J.C.J., & Olioso, A. (2007). Application of a simple algorithm to estimate daily evapotranspiration from NOAAAVHRR images for the Iberian Peninsula. *Remote Sensing of Environment*, 110, 139–148.
- Stathopoulou, M., & Cartalis, C. (2009). Downscaling AVHRR land surface temperatures for improved surface urban heat island intensity estimation. *Remote Sensing of Environment*, 113, 2592–2605.
- Vapnik, V.N. (1995). *The nature of statistical learning theory*. New York: Springer-Verlag.
- Verbeiren, S., Eerens, H., Piccard, I., Bauwens, I., & Van Orshoven, J. (2007). Sub-pixel classification of SPOT-VEGETATION time series for the assessment of regional crop areas in Belgium. *International Journal of Applied Earth Observation and Geoinformation*, 25, 45–57.
- Watkins, L.R. (2012). Review of fringe pattern phase recovery using the 1-D and 2-D continuous wavelet transforms. *Optics and Lasers in Engineering*, 50, 1015–1022.
- Weng, Q., Fu, P., & Gao, F. (2014). Generating daily land surface temperature at Landsat resolution by fusing Landsat and MODIS data. *Remote Sensing of Environment*, 145, 55–67.
- Yang, J., & Wang, Y. (2011). Estimating evapotranspiration fraction by modeling two-dimensional space of NDVI/albedo and day–night land surface temperature difference: a comparative study. *Advances in Water Resources*, 34, 512–518.
- Yu, X., Guo, X., & Wu, Z. (2014). Land surface temperature retrieval from Landsat 8 TIRS—comparison between radiative transfer equation-based method, Split Window Algorithm and Single Channel Method. *Remote Sensing*, 6, 9829–9852.
- Zhou, R., Bao, W., Li, N., Huang, X., & Yu, D. (2010). Mechanical equipment fault diagnosis based on redundant second generation wavelet packet transform. *Digital Signal Processing*, 20, 276–288.
- Zhu, X.L., Chen, J., Gao, F., Chen, X.H., & Masek, J.G. (2010). An enhanced spatial and temporal adaptive reflectance fusion model for complex heterogeneous regions. *Remote Sensing of Environment*, 114(11), 2610–2623.